Weierstraß-Institut

für Angewandte Analysis und Stochastik

Leibniz-Institut im Forschungsverbund Berlin e. V.

On a reduced sparsity stabilization of grad-div type for incompressible flow problems

Alexander Linke[1], Leo G. Rebholz[2]

submitted: August 2, 2013

[1] Weierstrass Institute
    Mohrenstr. 39
    10117 Berlin
    Germany
    email: Alexander.Linke@wias-berlin.de

[2] Clemson University
    Department of Mathematical Sciences
    Clemson, SC 29634
    USA
    email: rebholz@clemson.edu

Abstract

We introduce a new operator for stabilizing error that arises from the weak enforcement of mass conservation in finite element simulations of incompressible flow problems. We show this new operator has a similar positive effect on velocity error as the well-known and very successful grad-div stabilization operator, but the new operator is more attractive from an implementation standpoint because it yields a sparser block structure matrix. That is, while grad-div produces fully coupled block matrices (i.e. block-full), the matrices arising from the new operator are block-upper triangular in two dimensions, and in three dimensions the 2,1 and 3,1 blocks are empty. Moreover, the diagonal blocks of the new operator's matrices are identical to those of grad-div. We provide error estimates and numerical examples for finite element simulations with the new operator, which reveals the significant improvement in accuracy it can provide. Solutions found using the new operator are also compared to those using usual grad-div stabilization, and in all cases, solutions are found to be very similar.

1   Introduction

Weak enforcement of mass conservation in finite element simulations of incompressible flows is well known to cause instabilities and poor solution accuracy. Many methods have been developed that address this problem, including grad-div stabilization [22, 24], strongly divergence free finite element methods [5, 31, 7, 28, 1], and discontinuous Galerkin methods [5]. Of these methods, grad-div stabilization is likely attractive to the widest audience because it can easily be included into an existing conforming finite element code without adding any restrictions on elements or mesh type. As codes get older and bigger, making major changes can be a serious obstacle, but adding grad-div stabilization (or the related stabilization we propose herein) should not present major challenges, but can have a signicant positive impact on accuracy.

Although grad-div stabilization has seen significant interest and success in recent years [10, 22, 24, 19, 8, 6, 23], it also has a downside in its computational cost, although many believe it is often worth it for the gain in accuracy [25]. Although many common discretization methods for the Navier-Stokes equations (NSE) yield block diagonal matrices for the velocity components, the grad-div operator creates fully coupled matrices for velocity, which often makes solving the resulting linear algebraic systems more difficult. To address this issue, we propose and study a new

divergence stabilization operator that (we will show) has a similar positive effect on error as grad-div stabilization, but has a more efficient implementation because its matrices have a sparser block structure. The purpose of this paper is to introduce this new divergence penalization operator as a more efficient alternative to grad-div stabilization that it is simple to add it to an existing NSE (or similar) code, penalizes for lack of mass conservation, reduces the effect of the pressure error on the velocity error, and can dramatically improve accuracy. We introduce this new stabilization operator now.

Definition 1.1. *Let Ω be a bounded regular domain, and $u, v \in H^1(\Omega)^d$, $d = 2$ or 3. Define the divergence penalization operator g by*

$$g_{2d}(u, v) = \int_\Omega \left(u_{1_x} v_{1_x} + u_{2_y} v_{2_y} + 2 u_{2_y} v_{1_x} \right) \tag{1.1}$$

$$g_{3d}(u, v) = \int_\Omega \left(u_{1_x} v_{1_x} + u_{2_y} v_{2_y} + u_{3_z} v_{3_z} + 2 u_{2_y} v_{1_x} + 2 u_{3_z} v_{1_x} + u_{3_z} v_{2_y} + u_{2_y} v_{3_z} \right). \tag{1.2}$$

It is easy to observe that in g_{2d}, there is no interaction of the u_1 and v_2 functions, which means the resulting matrix is upper triangular. For g_{3d}, there is no interaction of u_1 with either v_2 or v_3, which means for the resulting 3x3 resulting block matrix, the 2,1 and 3,1 blocks are 0. This is in contrast to the grad-div stabilization operator

$$\text{grad-div}(u, v) = \int_\Omega (u_{1_x} + u_{2_y} + u_{3_z})(v_{1_x} + v_{2_y} + v_{3_z}),$$

which is block-full because each of u_1, u_2, and u_3 have interaction with each of v_1, v_2, and v_3.

The fundamental properties which allow the g operator to have a positive impact on incompressible flow simulations are provided in the following lemma. From here on, we denote the $L^2(\Omega)$ inner product by $(u, v) := \int_\Omega uv \, dx$.

Lemma 1.1. *The operator g has the following properties.*

1. *The operator g can be written as*

$$g_{2d}(u, v) = (\nabla \cdot u, \nabla \cdot v) - \left((u_{1_x}, v_{2_y}) - (u_{2_y}, v_{1_x}) \right), \tag{1.3}$$

$$g_{3d}(u, v) = (\nabla \cdot u, \nabla \cdot v) - \left((u_{1_x}, v_{2_y}) - (u_{2_y}, v_{1_x}) + (u_{1_x}, v_{3_z}) - (u_{3_z}, v_{1_x}) \right). \tag{1.4}$$

2. *Similar to grad-div stabilization, g satisfies in 2d or 3d,*

$$g(u, u) = \|\nabla \cdot u\|^2. \tag{1.5}$$

3. *If $\nabla \cdot u = 0$, then in 2d or 3d,*

$$g(u, v) = -(u_{1_x}, \nabla \cdot v). \tag{1.6}$$

Proof. To show (1.3), we add and subtract $u_{1_x} v_{2_y}$ to $g(u, v)$ in its definition (1.1), and group terms accordingly. For (1.4), we add and subtract $u_{1_x} v_{2_y}$ and $u_{1_x} v_{3_z}$, then regroup terms. For the equality (1.5), setting $v = u$ produces the result immediately.

2

To prove (1.6) for the 2d case, use use directly that $\nabla \cdot u = 0$ and that $u_{1_x} = -u_{2_y}$ to find

$$
\begin{aligned}
g_{2d}(u, v) &= (\nabla \cdot u, \nabla \cdot v) - \big((u_{1_x}, v_{2_y}) - (u_{2_y}, v_{1_x})\big) \\
&= -(u_{1_x}, v_{2_y}) + (u_{2_y}, v_{1_x}) \\
&= -(u_{1_x}, v_{2_y}) + (-u_{1_x}, v_{1_x}) \\
&= -(u_{1_x}, \nabla \cdot v)
\end{aligned}
$$

For (1.6) in the 3d case, a similar string of equalities that uses $u_{1_x} = -u_{2_y} - u_{3_z}$ provides

$$
\begin{aligned}
g_{3d}(u, v) &= (\nabla \cdot u, \nabla \cdot v) - \big((u_{1_x}, v_{2_y}) - (u_{2_y}, v_{1_x}) + (u_{1_x}, v_{3_z}) - (u_{3_z}, v_{1_x})\big) \\
&= -(u_{1_x}, v_{2_y}) + (u_{2_y}, v_{1_x}) - (u_{1_x}, v_{3_z}) + (u_{3_z}, v_{1_x}) \\
&= (u_{2_y} + u_{3_z}, v_{1_x}) - (u_{1_x}, v_{2_y}) - (u_{1_x}, v_{3_z}) \\
&= (-u_{1_x}, v_{1_x}) - (u_{1_x}, v_{2_y}) - (u_{1_x}, v_{3_z}) \\
&= -(u_{1_x}, \nabla \cdot v),
\end{aligned}
$$

which completes the proof. $\qquad\square$

The results and proofs from Lemma 1.1 reveal another interpretation of the g function: it is the resulting variational formulation of the sum of grad-div stabilization and the gradient of u_{1_x}, since for $v \in H_0^1(\Omega)$ and solenoidal u,

$$
-\nabla(\nabla \cdot u), v) + (\nabla u_{1_x}, v) = (\nabla \cdot u, \nabla \cdot v) - (u_{1_x}, \nabla \cdot v) = g(u, v).
$$

It is well known that gradient terms can be combined with the true pressure to create a modified pressure ($P = p + \gamma u_{1_x}$ in this case) that does not alter the velocity solution in the continuous case (for example, when computing with rotational form NSE, often the Bernoulli pressure $P_{Bernoulli} = p + |u|^2/2$ is used [12, 19]). Thus, the addition of g can be interpreted as grad-div stabilization together with a pressure alteration that creates a more efficient linear algebraic system for grad-div stabilization. We note that similar results can be achieved by using u_{2_y} or (in 3d) u_{3_z} instead of u_{1_x}, and still 2 blocks of the velocity matrix will be zero (but which 2 blocks will be different). It is intuitive, and revealed by our analysis, that if it is known which of u_{1_x}, u_{2_y}, u_{3_z} will be smallest, then this is the term that should be used to modify the pressure. Unfortunately, there does not appear to be any gradient term that can be added to the system in 3d that would yield a g operator that satisfies $g(u, u) = \|\nabla \cdot u\|^2$ and produces a block upper triangular matrix.

Although most of the common finite element discretization methods for the NSE have interactions of u_i with v_j only if $i = j$ (and so have block-diagonal velocity matrices), whether this difference in block structure between g and grad-div makes a significant difference in efficiency will depend on both the timestepping method and the solver. For Chorin-type projection methods (see, e.g. [25]), which use decoupled momentum equations with explicit pressure treatment, using g instead of grad-div will clearly provide for more efficient linear solves. For solvers that find velocity and pressure together, linear systems of the form

$$
\begin{pmatrix} A & B \\ B^T & 0 \end{pmatrix} \begin{pmatrix} U \\ P \end{pmatrix} = \begin{pmatrix} F \\ 0 \end{pmatrix}
$$

must be solved, with the A block representing the contributions of velocity with the momentum equations' test functions. In many discretizations (e.g. linearly extrapolated Crank-Nicolson [2]

which is studied herein), the A matrix will have a block-diagonal structure, and thus using grad-div will make A block-full while using g will lead to a block upper triangular matrix in 2d, or in 3d to a block matrix that has 2,1 and 3,1 blocks which are empty. Iterative solvers for these type of systems generally have two systems to (repeated solve/approximate), one with the A block and the other with the Schur complement. Compared to usual grad-div, using the proposed stabilization operator will simplify the A block solve but complicate the Schur complement, and hence it will require future studies to determine if/when the proposed stabilization operator will deliver an improvement over usual grad-div stabilization. In some preconditioners, simply by the nature of the factorization and approximations they are based on, grad-div may still be more appropriate, for example the modified Augmented Lagrangian type preconditioner of Benzi and Olshanskii [3] which has been shown quite successful [13], where usual grad-div stabilization can be considered an integral part of the theory of how the preconditioner works. In this case, there is often a tradeoff between the optimal grad-div stabilization parameters for accuracy and for efficiency, and here the use of the proposed g stabilization operator could offer an advantage since it stabilizes the divergence without adding the grad-div type augmentation to the linear algebraic system (i.e. the g operator could be used together with the augmentation, and have different parameters for stabilization and augmentation). Hence, from the solver point of view, there are many questions to be answered, most of which will be specific to individual solvers and preconditioners, and we leave this for future work.

Since the potential implementation advantage in many cases of g over grad-div is clear, it remains to show that the g operator does indeed have a positive effect on simulations (as grad-div stabilization does), and this paper is dedicated to showing it. In section 2, we give notation and preliminaries that will allow for a smooth analysis in the sections that follow. Section 3 gives a rigorous study of the new operator in the Stokes equations. Here, stability is proven, as is optimal convergence of both velocity and pressure. Numerical tests are provided that confirm the convergence rates, and that show using the new stabilization operator can have a significant positive influence on solution accuracy. In section 4, we extend the results to the case of the NSE. Here, we prove stability and optimal convergence of the stabilized linearly extrapolated Crank-Nicolson method, and give several more numerical examples that show how the use of g can improve solutions.

2 Notation and Preliminaries

In this section, we will present notation and mathematical preliminaries to allow for a smoother presentation in later sections.

For simplicity of analysis, we consider the domain $\Omega \subset \mathbb{R}^d$, $d = 2$ or 3, to be regular with piecewise smooth boundary. In our numerical experiments, we will also consider domains with holes (flow around a cylinder) and non-convex polygons (flow over a step). We will denote the L^2 inner product and norm by $(\cdot, \cdot)$ and $\|\cdot\|$, respectively. All other norms will be clearly labeled.

The natural velocity and pressure spaces for the Stokes and NSE are

$$
\begin{aligned}
X &:= \{v \in H^1(\Omega)^d, \ v|_{\partial\Omega} = 0\}, \\
Q &:= \{q \in L_0^2(\Omega), \ \int_\Omega q = 0\}.
\end{aligned}
$$

Denote by τ_h a regular, conforming mesh of Ω. Let $(X_h, Q_h) \subset (H_0^1(\Omega)^d, L_0^2(\Omega))$ be an LBB stable pair of finite element spaces defined on τ_h, and define the weakly and strongly divergence

4

free subspaces of X_h by V_h and $V_{h,0}$ by

$$
\begin{aligned}
V_h &:= \{v_h \in X_h, \ (\nabla \cdot v_h, q_h) = 0 \ \forall q_h \in Q_h\} \\
V_{h,0} &:= \{v_h \in X_h, \ \nabla \cdot v_h = 0\}
\end{aligned}
$$

We consider the space $V_{h,0}$ because in settings where this space has optimal approximation properties (see definition 2.1), our error analysis can be improved. Examples of such settings are the settings where Scott–Vogelius mixed finite elements satisfy the LBB condition, which includes the cases $X_h = P_k$ with $k \geq d$ on barycenter refined triangulations/tetrahedralizations [27, 1] and $k \geq d-1$ on Powell-Sabin grids [29, 30].

Definition 2.1 (Optimal approximation properties of the divergence-free subspace)**.** *Consider a sequence of quasi-uniform meshes with characteristic mesh size h and the corresponding spaces $V_{h,0}$ and X_h. If for all solenoidal $v \in X \cap H^{k+1}(\Omega)^d$,*

$$
\inf_{w_h \in V_{h,0}} \|\nabla v - \nabla w_h\| \leq C_{V_{h,0}} \inf_{w_h \in X_h} \|\nabla v - \nabla w_h\|
$$

with $C_{V_{h,0}}$ independent of h, then the sequence of spaces $V_{h,0}$ is said to possess optimal approximation properties.

3   A new divergence stabilization method for finite element approximations of the Stokes equations

For simplicity, we consider first finite element approximations to the incompressible Stokes equations with the new divergence stabilization term. The positive effects of the new divergence stabilization term can be shown in this case, and the analysis developed here will extend to timestepping methods for the NSE in the next section.

The incompressible Stokes equations under homogeneous Dirichlet boundary conditions are given by

$$
\begin{aligned}
-\nu \Delta u + \nabla p &= f, & (3.1) \\
\nabla \cdot u &= 0, & (3.2) \\
u|_{\partial \Omega} &= 0, & (3.3) \\
\int_\Omega p \, dx &= 0. & (3.4)
\end{aligned}
$$

The purpose of studying the operator g together with Stokes is that this is a simplest setting to analyze the behavior of g. It is our ultimate intention to use the operator in finite element approximations for NSE flows, where it is well known that grad-div stabilization can make a dramatic improvement in solution accuracy.

3.1   A discrete stabilized Stokes algorithm and its well-posedness

We now define a stabilized algorithm for Stokes, based on the use of g.

Algorithm 3.1 (Stokes with new divergence stabilization operator)*. For a given stabilization parameter $\gamma > 0$, the stabilized finite element formulation of the Stokes equations studied herein is given by: Find $(u_h, p_h) \in (X_h, Q_h)$ satisfying*

$$\nu(\nabla u_h, \nabla v_h) - (p_h, \nabla \cdot v_h) + \gamma g(u_h, v_h) = (f, v_h) \quad \forall v_h \in X_h, \tag{3.5}$$

$$(\nabla \cdot u_h, q_h) = 0 \ \forall q_h \in Q_h. \tag{3.6}$$

We note that $p_h + \gamma(u_h)_{1_x}$ represents an approximation to the true Stokes pressure, and we will prove below that this 'modified pressure' converges optimally to the true Stokes pressure. The pressure p_h in Algorithm 3.1 does not represent an approximation to the Stokes pressure, since as is discussed in the introduction, the use of g implicitly creates a modified pressure.

For analysis purposes, we will also consider the V_h formulation of (3.5)-(3.6): Find $u_h \in V_h$ satisfying

$$\nu(\nabla u_h, \nabla v_h) + \gamma g(u_h, v_h) = (f, v_h) \quad \forall v_h \in V_h. \tag{3.7}$$

With (X_h, Q_h) satisfying the LBB condition, the formulations (3.7) and (3.5)-(3.6) are equivalent.

We begin our analysis by proving (3.7) is stable and well-posed.

Lemma 3.1. *Solutions to the Algorithm 3.1 (the discrete Stokes approximation) exist uniquely, and satisfy*

$$\nu \|\nabla u_h\|^2 + 2\gamma \|\nabla \cdot u_h\|^2 \le \nu^{-1} \|f\|_{-1}^2. \tag{3.8}$$

Remark 3.1. *From (3.8), we observe that stabilization using the g operator with the parameter γ provides control over the divergence error.*

Proof. Starting from the V_h formulation (3.7), we note that this system is linear and finite dimensional, so proving the stability estimate (3.8) will also imply that solutions exist uniquely. Choosing $v_h = u_h$ in (3.7) yields

$$\nu \|\nabla u_h\|^2 + \gamma g(u_h, u_h) = (f, u_h).$$

From (1.5), $g(u_h, u_h) = \|\nabla \cdot u_h\|^2$, and using this and majorizing the right hand size in the usual way gives us

$$\frac{\nu}{2} \|\nabla u_h\|^2 + \gamma \|\nabla \cdot u_h\|^2 \le \frac{\nu^{-1}}{2} \|f\|_{-1}^2.$$

Multiplying both sides by 2 finishes the proof. $\qquad \square$

3.2 Error analysis

Here, we prove optimal convergence of both the velocity and a modified pressure in the stabilized Stokes algorithm of Algorithm 3.1. We begin with the velocity error, as the pressure error will depend on the velocity error.

Theorem 3.1 (Optimal velocity convergence)*. Let (u, p) solve the Stokes problem (3.1)-(3.4). Then the velocity error in Algorithm 3.1 satisfies*

$$\nu \|\nabla(u - u_h)\|^2 + \gamma \|\nabla \cdot (u - u_h)\|^2 \le$$
$$C\left((\nu + \gamma^2 \nu^{-1}) \inf_{w_h \in X_h} \|\nabla(u - w_h)\|^2 + \gamma^{-1} \inf_{q_h \in Q_h} \|(p - \gamma u_{1_x}) - q_h\|^2 \right). \tag{3.9}$$

6

Remark 3.2. *If $(X_h, Q_h) = ((P_k)^d, P_{k-1})$ elements, then convergence of algorithm (3.7) is easily seen to be asymptotically optimal. By standard approximation theory [4], we have that*

$$\nu \|\nabla(u - u_h)\|^2 + \gamma \|\nabla \cdot (u - u_h)\|^2 \le Ch^{2k} \left((\nu + \gamma^2 \nu^{-1}) |u|_{k+1}^2 + \gamma^{-1} |(p - \gamma u_{1_x})|_k^2 \right). \qquad (3.10)$$

Remark 3.3. *Without the use of g, the standard error estimate for Stokes has the form [18]*

$$\nu \|\nabla(u - u_h)\|^2 \le C \left(\nu \inf_{w_h \in X_h} \|\nabla(u - w_h)\|^2 + \nu^{-1} \inf_{q_h \in Q_h} \|(p - q_h\|^2) \right). \qquad (3.11)$$

This estimate and that of Theorem 3.1 suggest that the g operator acts to reduce the effect of the pressure discretization error on the velocity error, but increases the effect of the velocity discretization error. Particularly for the cases of large, complex pressures (relative to velocities) and small viscosities, the error estimate provided by the use of g appears quite advantageous. We also note that the scaling of the error with γ suggests that it will most often be the case that good choices of γ will be $O(1)$ or smaller.

Proof. We begin by multiplying the Stokes equations by $v_h \in V_h$, and integrating by parts. Next, add $\gamma g(u, v_h)$ to both sides of the equation, and since $\nabla \cdot u = 0$, use property (1.6) of g on the right hand side of the equation to get

$$\nu(\nabla u, \nabla v_h) - (p, \nabla \cdot v_h) + \gamma g(u, v_h) = (f, v_h) - \gamma(u_{1_x}, \nabla \cdot v_h) \ \forall v_h \in V_h.$$

Subtracting from this the V_h form of the stabilized Stokes approximation (3.7), then and writing $e = u - u_h$, we get

$$\nu(\nabla e, \nabla v_h) + \gamma g(e, v_h) = (p - \gamma u_{1_x}, \nabla \cdot v_h) \ \forall v_h \in V_h.$$

Since $v_h \in Q_h$, we have that for any $q_h \in Q_h$,

$$\nu(\nabla e, \nabla v_h) + \gamma g(e, v_h) = (p - \gamma u_{1_x} - q_h, \nabla \cdot v_h) \ \forall v_h \in V_h.$$

Next, we write $e = (u - w_h) + (w_h - u_h) =: \eta + \phi_h$, where $w_h \in V_h$ is arbitrary. Using this decomposition, and choosing $v_h = \phi_h$ gives

$$\nu \|\nabla \phi_h\|^2 + \gamma \|\nabla \cdot \phi_h\|^2 = -\nu(\nabla \eta, \nabla \phi_h) - \gamma g(\eta, \phi_h) + ((p - \gamma u_{1_x}) - q_h, \nabla \cdot \phi_h), \qquad (3.12)$$

and applying Cauchy-Schwarz and Young's inequalities provides

$$\frac{\nu}{2} \|\nabla \phi_h\|^2 + \frac{\gamma}{2} \|\nabla \cdot \phi_h\|^2 \le \frac{\nu}{2} \|\nabla \eta\|^2 - \gamma g(\eta, \phi_h) + \frac{\gamma^{-1}}{2} \inf_{q_h \in Q_h} \|(p - \gamma u_{1_x}) - q_h\|^2. \qquad (3.13)$$

To bound the g function on the right hand side, we use

$$|\gamma g(\eta, \phi_h)| \le C\gamma \|\nabla \eta\| \|\nabla \phi_h\| \le \frac{\nu}{4} \|\nabla \phi_h\|^2 + C\nu^{-1} \gamma^2 \|\nabla \eta\|^2,$$

and combining this with (3.13) and reducing gives the estimate

$$\nu \|\nabla \phi_h\|^2 + \gamma \|\nabla \cdot \phi_h\|^2 \le C \left((\nu + \nu^{-1} \gamma^2) \|\nabla \eta\|^2 + \gamma^{-1} \inf_{q_h \in Q_h} \|(p - \gamma u_{1_x}) - q_h\|^2 \right).$$

Applying the triangle inequality and using the assumption of LBB on (X_h, Q_h) to change the infimum to be over X_h instead of V_h, completes the proof. $\qquad \square$

7

Next, we prove optimal convergence of a modified pressure $p_h + \gamma(u_h)_{1_x}$ from Algorithm 3.1 to the true Stokes pressure.

Theorem 3.2 (Optimal convergence of a modified pressure). *Let (u, p) solve the Stokes problem (3.1)-(3.4). The pressure error in the approximation (u_h, p_h) from Algorithm 3.1 satisfies*

$$\|p - (p_h + \gamma(u_h)_{1_x})\| \leq$$
$$C\left((1 + \frac{\nu^{1/2}}{\gamma^{1/2}} + \frac{\gamma^{1/2}}{\nu^{1/2}}) \inf_{r_h \in Q_h} \|(p - \gamma u_{1_x}) - r_h\| + (\nu^{1/2}\gamma + \nu^{3/2} + \gamma^2\nu^{-1/2}) \inf_{w_h \in X_h} \|\nabla(u - w_h)\|\right).$$
$$(3.14)$$

Remark 3.4. *If $(X_h, Q_h) = ((P_k)^d, P_{k-1})$ elements, then convergence of algorithm (3.7) is easily seen to be asymptotically optimal. By standard approximation theory [4]*

$$\|p - (p_h + \gamma(u_h)_{1_x})\| \leq Ch^k\left((1 + \frac{\nu^{1/2}}{\gamma^{1/2}} + \frac{\gamma^{1/2}}{\nu^{1/2}})|p - \gamma u_{1_x}|_k + (\nu + \gamma + \gamma^2\nu^{-1})|u|_{k+1}\right). \quad (3.15)$$

Proof. Similar to the beginning of the proof of Theorem 3.1, we have that for $v_h \in X_h$, the true Stokes solution satisfies

$$\nu(\nabla u, \nabla v_h) - (p - \gamma u_{1_x}, \nabla \cdot v_h) + \gamma g(u, v_h) = (f, v_h).$$

Subtracting (3.5) from this gives the error equation

$$((p - \gamma u_{1_x}) - p_h, \nabla \cdot v_h)) = \nu(\nabla e, \nabla v_h) + \gamma g(e, v_h) \ \forall v_h \in X_h. \quad (3.16)$$

Next, adding and subtracting an arbitrary $r_h \in Q_h$ in the pressure term gives

$$(r_h - p_h, \nabla \cdot v_h) = -((p - \gamma u_{1_x}) - r_h, \nabla \cdot v_h) + \nu(\nabla e, \nabla v_h) + \gamma g(e, v_h) \ \forall v_h \in X_h,$$

and then applying the Cauchy-Schwarz inequality, using $\|\nabla \cdot v_h\| \leq \|\nabla v_h\|$, and dividing both sides by $\|\nabla v_h\|$ provides the equation

$$\frac{(r_h - p_h, \nabla \cdot v_h)}{\|\nabla v_h\|} = \|(p - \gamma u_{1_x}) - r_h\| + \nu\|\nabla e\| + \gamma\frac{g(e, v_h)}{\|\nabla v_h\|}. \quad (3.17)$$

Bounding g as in the velocity convergence proof, taking the supremum over $v_h \in X_h$ and applying LBB now gives

$$\|r_h - p_h\| \leq C\left(\|(p - \gamma u_{1_x}) - r_h\| + (\nu + \gamma)\|\nabla e\|\right), \quad (3.18)$$

and thus by the triangle inequality,

$$\|(p - \gamma u_{1_x}) - p_h\| \leq C\left(\|(p - \gamma u_{1_x}) - r_h\| + (\nu + \gamma)\|\nabla e\|\right). \quad (3.19)$$

Again using the triangle inequality, along with (3.19), we have that

$$\begin{aligned}
\|p - (p_h + \gamma(u_h)_{1_x})\| &= \|p - \gamma u_{1_x} + \gamma u_{1_x} - p_h - \gamma(u_h)_{1_x}\| \\
&\leq \|p - \gamma u_{1_x} - p_h\| + \gamma\|e_{1_x}\| \\
&\leq C\left(\|(p - \gamma u_{1_x}) - r_h\| + (\nu + \gamma)\|\nabla e\|\right). \quad (3.20)
\end{aligned}$$

Taking the infimum over all $r_h \in Q_h$, then using the results of Theorem 3.1 finishes the proof. $\square$

3.3 Error analysis in the special case that $V_{h,0}$ has optimal approximation properties

In certain finite element settings, depending on the mesh type and approximating polynomial degree of the velocity space, the pointwise divergence free subspace of the velocity space can have optimal approximation properties (see definition 2.1). The advantage of such spaces with regards to analysis of Algorithm 3.1 is that here we can get an improved estimate of the term $\gamma g(\eta, \phi_h)$ in the velocity error estimate, which will reduce the poor scaling of the error with larger γ in Theorem 3.1. We now prove error estimates for the velocity and pressure in the case that $V_{h,0}$ has optimal approximation properties.

Theorem 3.3. *Let (u, p) solve the Stokes problem (3.1)-(3.4). If $V_{h,0}$ has optimal approximation properties, then the velocity error in Algorithm 3.1 is bounded by*

$$\nu \left\| \nabla(u - u_h) \right\|^2 + \gamma \left\| \nabla \cdot (u - u_h) \right\|^2 \leq$$
$$C \left((\nu + \gamma) \inf_{w_h \in X_h} \left\| \nabla(u - w_h) \right\|^2 + \gamma^{-1} \inf_{q_h \in Q_h} \left\| p - \gamma u_{1_x} - q_h \right\|^2 \right), \quad (3.21)$$

and the pressure error satisfies

$$\left\| p - (p_h + \gamma(u_h)_{1_x}) \right\| \leq$$
$$C \left((1 + \frac{\nu^{1/2}}{\gamma^{1/2}} + \frac{\gamma^{1/2}}{\nu^{1/2}}) \inf_{r_h \in Q_h} \left\| (p - \gamma u_{1_x}) - r_h \right\| + (\nu^{1/2}\gamma^{1/2} + \nu + \gamma + \gamma^{3/2}\nu^{-1/2}) \inf_{w_h \in X_h} \left\| \nabla(u - w_h) \right\| \right).$$
$$(3.22)$$

Remark 3.5. *The gain from requiring the space $V_{h,0}$ to have optimal approximation properties is that the coefficients in the error bounds are smaller than in the general case if γ is taken to be larger than 1. Of course, comparing errors by comparing respective upper bounds does not necessarily provide a good comparison. In the general case, since $\nabla \cdot \eta$ is expected small in some sense, the bound we use in the proof of Theorem 3.1 may be pessimistic.*

Proof. The proof follows that of Theorem 3.1 almost exactly up to (3.13), with the only difference being that we take w_h arbitrary in $V_{h,0}$. This gives that $\nabla \cdot \eta = 0$, and with this in mind, we start from (3.13), which is the relation

$$\frac{\nu}{2} \left\| \nabla \phi_h \right\|^2 + \frac{\gamma}{2} \left\| \nabla \cdot \phi_h \right\|^2 \leq \frac{\nu}{2} \left\| \nabla \eta \right\|^2 - \gamma g(\eta, \phi_h) + \frac{\gamma^{-1}}{2} \inf_{q_h \in Q_h} \left\| (p - \gamma u_{1_x}) - q_h \right\|^2. \quad (3.23)$$

we can now bound the g term with

$$\left| \gamma g(\eta, \phi_h) \right| = \left| \gamma(\eta_{1_x}, \nabla \cdot \phi_h) \right| \leq \frac{\gamma}{4} \left\| \nabla \cdot \phi_h \right\|^2 + 2\gamma \left\| \nabla \eta \right\|^2.$$

and combining this with (3.23) and reducing gives the estimate

$$\nu \left\| \nabla \phi_h \right\|^2 + \gamma \left\| \nabla \cdot \phi_h \right\|^2 \leq C \left((\nu + \gamma) \left\| \nabla \eta \right\|^2 + \gamma^{-1} \inf_{q_h \in Q_h} \left\| (p - \gamma u_{1_x}) - q_h \right\|^2 \right).$$

Applying the triangle inequality and using the assumption of LBB on (X_h, Q_h) completes the proof for velocity. For the pressure estimate, we simply combine this new velocity error bound with the last step of the proof of the pressure error estimate of Theorem 3.2. $\square$

3.4 Numerical experiments for Stokes

Here we test the predicted convergence rates of Theorems 3.1 and 3.2, both in 2d and 3d, and then for a test problem with smaller viscosity and larger pressure, we compare errors found by the proposed stabilized method, an unstabilized method, and a method using usual grad-div stabilization.

3.4.1 Convergence rate verification for 2d test problem

We now test the predicted optimal convergence rates of Algorithm 3.1 on an analytical test problem. The solution is given on $\Omega = (0,1)^2$ by

$$
\begin{aligned}
u_1(x,y) &= \sin(\pi x)\cos(\pi y), \\
u_2(x,y) &= -\sin(\pi y)\cos(\pi x), \\
p(x,y) &= \sin(\pi(x+2y)).
\end{aligned}
$$

We choose $\nu = 1$, and calculate f from the Stokes equations. We compute using $((P_2)^2, P_1)$ Taylor-Hood elements with Algorithm 3.1 and $\gamma = 1$, on successively refined uniform triangular meshes. Dirichlet boundary conditions for velocity are enforced so that the computed solution interpolates the true solution at the boundary nodes. $H^1(\Omega)$ errors and convergence rates for velocity, and $L^2(\Omega)$ errors and convergence rates for modified pressure, are shown in Table 1. We observe the convergence rates are optimal, as predicted by the theory.

h	dof	$\|u - u_h\|_1$	Rate	$\|p - (p_h + \gamma(u_h)_{1_x})\|$	Rate
1/4	162	1.9859e-1	-	1.9610e-1	-
1/8	578	4.8390e-2	2.037	4.2442e-2	2.208
1/16	2,178	1.1985e-2	2.014	1.0106e-2	2.070
1/32	8,450	2.9883e-3	2.004	2.4949e-3	2.018
1/64	33,282	7.4658e-4	2.001	6.2175e-4	2.005
1/128	132,098	1.8661e-4	2.000	1.5531e-4	2.001

Table 1: H^1 Velocity and L^2 pressure errors and rates for the proposed stabilized Stokes system for the 2d test problem. We observe optimal convergence for both.

3.4.2 Convergence rate verification for 3d test problem

We now test the predicted optimal convergence rates of Algorithm 3.1 on a 3d analytical test problem. The solution is given on $\Omega = (0,1)^3$ by

$$
\begin{aligned}
u_1(x,y,z) &= \cos(2\pi z), \\
u_2(x,y,z) &= \sin(2\pi x), \\
u_3(x,y,z) &= \sin(2\pi y), \\
p(x,y,z) &= \sin(2\pi(x+y+z)).
\end{aligned}
$$

Again, we choose $\nu = 1$, and calculate f from the Stokes equations. We compute in 3d using $((P_2)^3, P_1)$ Taylor-Hood elements with Algorithm 3.1, and $\gamma = 1$, on successively refined uniform tetrahedral meshes. Dirichlet boundary conditions for velocity are enforced so that the computed

solution interpolates the true solution at the boundary nodes. $H^1(\Omega)$ errors and convergence rates for velocity, and $L^2(\Omega)$ errors and convergence rates for modified pressure, are shown in Table 2 for the computations on the varying meshes. We observe the convergence rates are optimal, as predicted by the theory.

h	dof	$\|u - u_h\|_1$	Rate	$\|p - (p_h + \gamma(u_h)_{1_x})\|$	Rate
1/4	2,312	6.812e-1	-	1.951e-1	-
1/8	15,468	1.751e-1	1.960	4.216e-2	2.210
1/12	49,072	7.827e-2	1.993	1.818e-2	2.0751
1/16	112,724	4.411e-2	1.990	1.011e-2	2.040
1/20	216,024	2.826e-2	1.978	6.430e-3	2.206
1/24	368,572	1.964e-2	2.015	4.453e-3	2.016
1/32	859,812	1.105e-2	2.000	2.499e-3	2.008

Table 2: H^1 Velocity and L^2 pressure errors and rates for the proposed stabilized Stokes system for the 3d test problem. We observe optimal convergence.

3.4.3 Error comparison for a test problem with smaller ν and larger pressure

We next compare errors found by Algorithm 3.1 using $\gamma = 1$ with those found using no stabilization (i.e. $\gamma = 0$), and those found using usual grad-div stabilization (with stabilization parameter of 1). We use a similar test problem and setup as for the 2d convergence rates test, but here we take $\nu = 0.01$ and true pressure solution

$$p(x,y) = 100\sin(\pi(x + 2y)).$$

From our analysis, this is a case when it is expected that the stabilization operator will increase accuracy. $H^1(\Omega)$ velocity errors and $L^2(\Omega)$ divergence and pressure errors are displayed in Figure 3. Although each method converges optimally (rates not shown), we observe the stabilized methods have an order of magnitude less error in the $H^1(\Omega)$ norm, and two orders of magnitude decrease in the $L^2(\Omega)$ norm of the divergence error, compared to the unstabilized method. The errors in the pressures are about the same for all the methods. Also, we observe the errors of the proposed stabilization and grad-div stabilization methods' solutions are very close.

h	$\|u - u_h\|_1$	$\|\nabla \cdot u_h\|$	$\|p - \widetilde{p_h}\|$	$\|u - u_h\|_1$	$\|\nabla \cdot u_h\|$	$\|p - p_h\|$	$\|u - u_h\|_1$	$\|\nabla \cdot u_h\|$	$\|p - p_h\|$
$\frac{1}{4}$	2.80e1	9.17e0	1.33e1	2.99e1	1.08e1	1.46e1	9.81e2	9.53e2	1.47e1
$\frac{1}{8}$	6.93e0	1.33e0	2.86e0	8.38e0	1.60e0	3.10e0	1.36e2	1.33e2	3.11e0
$\frac{1}{16}$	1.16e0	1.78e-1	7.07e-1	1.78e0	2.10e-1	7.28e-1	1.76e1	1.73e1	7.28e-1
$\frac{1}{32}$	1.68e-1	2.29e-2	1.78e-1	2.98e-1	2.51e-2	1.78e-1	2.24e0	2.21e0	1.78e-1
$\frac{1}{64}$	2.25e-2	2.92e-3	4.45e-2	4.21e-2	2.99e-3	4.45e-2	2.83e-1	2.79e-1	4.45e-2
$\frac{1}{128}$	2.90e-3	3.85e-4	1.11e-2	5.54e-3	3.81e-4	1.11e-2	3.56e-2	3.51e-2	1.11e-2

Table 3: Velocity, divergence, and pressure errors for the proposed stabilized method, grad-div stabilized method, and unstabilized method, on various meshes. In the table, we use $\widetilde{p_h} = (p_h + \gamma(u_h)_{1_x})$.
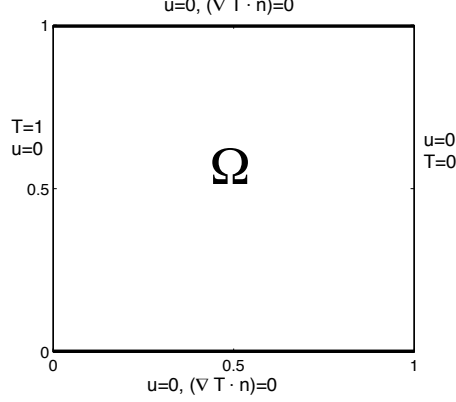
Figure 1: The domain and boundary conditions for the Rayleigh–Bénard convection problem.

3.5 Numerical test for Rayleigh–Bénard convection for silicon oil

The next test problem we study is the differentially heated cavity with Rayleigh number Ra=10^6, and Prandtl number Pr= ∞ (corresponding to silicon oil), using the unit square as the domain, with boundary conditions for the velocity taken to be no-slip, and mixed Dirichlet/Neumann conditions for temperature, see Figure 1. Although this system is modeled by the Boussinesq equations, with Pr=∞, the momentum equations are reduced to a Stokes equation with a forcing $f = \langle 0, RaT \rangle^T$, and so it is appropriate to study this system in the context of approximating Stokes.

A standard finite element approach, see, e.g., [11], is to use $(X_h, Q_h) = ((P_2)^2, P_1)$ Taylor–Hood elements for velocity and pressure, and P_2 to approximate the temperature. The finite element formulation, together with our proposed stabilization, for a specified Ra takes the form: Find $(u_h, p_h, T_h - T_{d,h}) \in X_h \times Q_h \times X_h^{1d}$ such that for all $(v_h, q_h, s_h) \in X_h \times Q_h \times X_h^{1d}$

$$(\nabla u_h, \nabla v_h) + \gamma g(u_h, v_h) - (\nabla \cdot v_h, p_h) = ((0, Ra\ T_h)^{\mathrm{T}}, v_h),$$
$$(\nabla \cdot u_h, q_h) = 0, \tag{3.24}$$
$$(\nabla T_h, \nabla s_h) + (u_h \cdot \nabla T_h, s_h) = 0,$$

where $T_{d,h}$ is an extension of the Dirichlet data to the finite element space with inhomogeneous Dirichlet boundary conditions. The nonlinearity of (3.24) is resolved to a relative difference of 10^{-10} in successive iterates using Newton's method. We used a continuation method in Ra to get convergence $Ra = 10^6$, via Ra $\in \{10^4, 10^5, 10^6\}$. Plots of the resolved solution's velocity streamlines and temperature contours are shown in Figure 2. This solution was found using a Delaunay mesh that provided 47,644 total degrees of freedom with $((P_2)^2, P_1, P_2)$ elements, and using $\gamma = 0$. We note this resolved solution matches the one found in [16] very well.

To illustrate the positive effects of the proposed stabilization operator, we computed solutions to (3.24), again using $((P_2)^2, P_1, P_2)$ elements for velocity-pressure-temperature, but now on a much coarser Delaunay triangulation that provided only 9,893 total degrees of freedom, and using $\gamma = 0$ and 10 (the larger γ was optimal for this problem, which is not surprising since large divergence stabilization is known to help heated cavity simulations [16, 8]). Solutions are shown in Figure 3, and it is clear to observe that the stabilized solution does a better job approximating the streamlines near the center of the cavity.
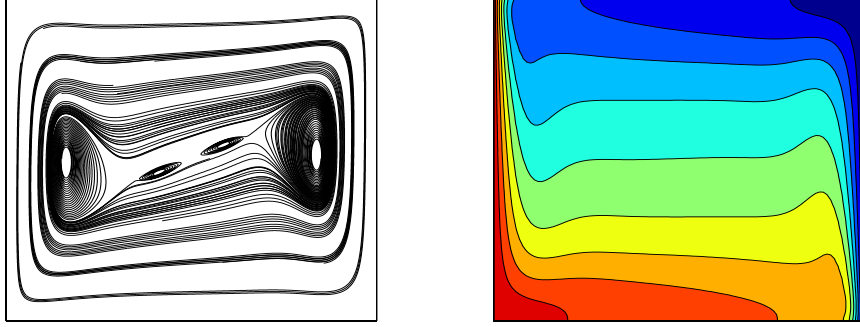
Figure 2: Shown above are the resolved solution's velocity streamlines and temperature contours.
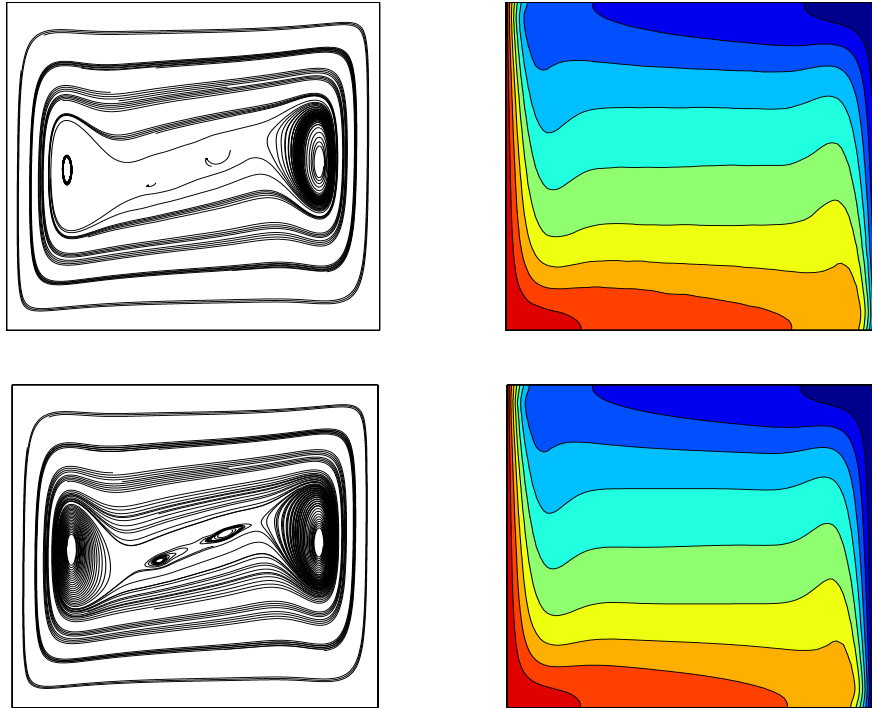

Figure 3: Shown above are the coarser mesh solutions' velocity streamlines and temperature contours for $\gamma = 0$ (top) and $\gamma = 10$ (bottom).

4 A new divergence stabilization method for finite element approximations of the Navier-Stokes equations

In this section, we extend analysis and testing of the divergence stabilization operator g to finite element discretizations of the time dependent, incompressible NSE, which are given in the case of

wall bounded flows by

$$u_t + u \cdot \nabla u - \nu \Delta u + \nabla p = f, \tag{4.1}$$
$$\nabla \cdot u = 0, \tag{4.2}$$
$$u|_{\partial \Omega} = 0, \tag{4.3}$$
$$u(0, x) = u_0, \tag{4.4}$$
$$\int_\Omega p \ dx = 0. \tag{4.5}$$

Define the skew-symmetric operator $b^* : X \times X \times X \to \mathbb{R}$ by

$$b^*(u, v, w) = \frac{1}{2}(u \cdot \nabla v, w) - \frac{1}{2}(u \cdot \nabla w, v)$$

If $\nabla \cdot u = 0$, then $b^*(u, v, w) = (u \cdot \nabla v, w)$, and no matter the divergence of u, $b^*(u, v, v) = 0$.

Consider the linearly extrapolated Crank-Nicolson in time, finite element in space algorithm for approximating solutions to the NSE (i.e. the method of Baker [2]). The system (4.6)-(4.7) is an example of a system which has a block-diagonal velocity matrix if $\gamma = 0$. We denote the average of the n and n+1st timesteps by

$$\phi^{n+1/2} := \frac{\phi^n + \phi^{n+1}}{2}.$$

Algorithm 4.1. *Given $u_h^0 \in V_h$, $f \in L^\infty(0, T; H^{-1}(\Omega))$, end time T, timestep $\Delta t = \frac{T}{M}$, for n=1,2,...,M-1, find $(u_h^{n+1}, p_h^{n+1}) \in (X_h, Q_h)$ satisfying $\forall (v_h, q_h) \in (X_h, Q_h)$,*

$$\frac{1}{\Delta t}(u_h^{n+1} - u_h^n, v_h) + b^* \left(\frac{3}{2}u_h^n - \frac{1}{2}u_h^{n-1}, u_h^{n+1/2}, v_h \right) + \nu(\nabla u_h^{n+1/2}, \nabla v_h)$$
$$-(p^{n+1/2}, \nabla \cdot v_h) + \gamma g(u_h^{n+1/2}, v_h) = (f(t^{n+1/2}), v_h) \tag{4.6}$$
$$(\nabla \cdot u_h^{n+1}, q_h) = 0. \tag{4.7}$$

We note the initial pressure p_h^0 is not needed. Second order temporal accuracy can be maintained if the first timestep is taken using backward Euler, and then Crank-Nicolson is used for subsequent timesteps. Alternatively, one may solve for $p_h^{n+1/2}$ directly, and interpret the solution as the pressure approximation to $p(t^{n+1/2})$.

Due to the assumption that (X_h, Q_h) satisfies LBB, the system (4.6)-(4.7) is equivalent to the V_h formulation at each timestep: Find $u_h^{n+1} \in V_h$ satisfying

$$\frac{1}{\Delta t}(u_h^{n+1} - u_h^n, v_h) + b^* \left(\frac{3}{2}u_h^n - \frac{1}{2}u_h^{n-1}, u_h^{n+1/2}, v_h \right) + \nu(\nabla u_h^{n+1/2}, \nabla v_h)$$
$$+ \gamma g(u_h^{n+1/2}, v_h) = (f(t^{n+1/2}), v_h) \ \forall v_h \in V_h. \tag{4.8}$$

4.1   Analysis of the stabilized algorithm for NSE

Lemma 4.1. *Solutions to Algorithm 4.1 exist uniquely, and satisfy*

$$\left\| u_h^M \right\|^2 + \nu \Delta t \sum_{n=0}^{M-1} \left\| \nabla u_h^{n+1/2} \right\|^2 + \gamma \Delta t \sum_{n=0}^{M-1} \left\| \nabla \cdot u_h^{n+1/2} \right\|^2 \leq \left\| u_h^0 \right\|^2 + \nu^{-1} \Delta t \sum_{n=0}^{M-1} \left\| f(t^{n+1/2}) \right\|_{-1}^2. \tag{4.9}$$

Proof. We begin by proving estimate (4.9). Let $u_h^n \in V_h$, n=0,1,2,...,M be a velocity solution to Algorithm 4.1. Setting $v_h = u_h^{n+1/2}$ in (4.8) vanishes the nonlinear term, and then applying Lemma 1.1 yields

$$\frac{1}{2}(\|u_h^{n+1}\|^2 - \|u_h^n\|^2) + \nu \left\|\nabla u_h^{n+1/2}\right\|^2 + \gamma \left\|\nabla \cdot u_h^{n+1/2}\right\|^2 \;=\; (f(t^{n+1/2}), u_h^{n+1/2})$$

$$\leq\; \frac{\nu}{2}\left\|\nabla u_h^{n+1/2}\right\|^2 + \frac{\nu^{-1}}{2}\|f\|_{-1}^2\,.$$

From here, reducing and summing over timesteps proves (4.9) for any solution of Algorithm 4.1. This result immediately proves that solutions at each timestep must be unique, and since the problem is linear and finite dimensional at each timestep, existence and uniqueness of solutions follows. $\qquad\square$

Theorem 4.1. *Let (u, p) be a sufficiently smooth NSE solution, so that the norms on the right hand side of* (4.10) *exist . The velocity error in approximating NSE with Algorithm 4.1 is bounded by*

$$\left\|u(T) - u_h^M\right\|^2 + \nu\Delta t \sum_{n=0}^{M-1} \left\|\nabla(u(t^{n+1/2}) - u_h^{n+1/2})\right\|^2 + \gamma\Delta t \sum_{n=0}^{M-1} \left\|\nabla \cdot u_h^{n+1/2}\right\|^2 \leq$$

$$C\left((\nu + \gamma^2\nu^{-1} + \nu^{-1} + \nu^{-2})\,\||u(t)|_k\|_{L^\infty(0,T)}^2\,h^{2k} + \gamma^{-1}\,\||p(t) - \gamma u_{1_x}(t)|_k\|_{L^\infty(0,T)}^2\,h^{2k} + C\Delta t^4\right) \tag{4.10}$$

Remark 4.1. *If the stabilization had not been used, the error estimate becomes*

$$\left\|u(T) - u_h^M\right\|^2 + \nu\Delta t \sum_{n=0}^{M-1} \left\|\nabla(u(t^{n+1/2}) - u_h^{n+1/2})\right\|^2 \leq$$

$$C\left((\nu + \nu^{-1} + \nu^{-2})\,\||u(t)|_k\|_{L^\infty(0,T)}^2\,h^{2k} + \nu^{-1}\,\||p(t)|_k\|_{L^\infty(0,T)}^2\,h^{2k} + C\Delta t^4\right) \tag{4.11}$$

Thus we see that for smaller ν, the use of the proposed stabilization operator g reduces the effect of the pressure discretization error on the velocity error. Moreover, for $\nu \ll \gamma \leq O(1)$, comparing the estimates suggests the new stabilization operator does not appear to provide any negative influence on the solution.

Proof. Denote $u^n := u(t^n)$ for the NSE velocity solution at time $t = t^n$, for n=0,1,2,...,M, and note that $u^{n+1/2}$ is not necessarily equal to $1/2(u^n + u^{n+1})$. Similar to Stokes analysis of section 3, we multiply the NSE by $v_h \in V_h$, then add $\gamma g(u^{n+1/2}, v_h)$ to both sides, reduce the right hand side with $\gamma g(u^{n+1/2}, v_h) = (-\gamma u_{1_x}^{n+1/2}, \nabla \cdot v_h)$, and subtract off the discrete scheme (4.8) to get

$$\frac{1}{\Delta t}(e^{n+1} - e^n, v_h) + \nu(\nabla e^{n+1/2}, \nabla v_h) + \gamma g(e^{n+1/2}, v_h) = -(p(t^{n+1/2}) - \gamma u_{1_x}^{n+1/2}, \nabla \cdot v_h)$$

$$- b^*\left(\frac{3}{2}u_h^n - \frac{1}{2}u_h^{n-1}, e^{n+1/2}, v_h\right) - b^*\left(\frac{3}{2}e^n - \frac{1}{2}e^{n-1}, u^{n+1/2}, v_h\right) - \Phi(n, v_h), \tag{4.12}$$

where $e^n := u^n - u_h^n$ and

$$\Phi(n, v_h) := \left(u_t(t^{n+1/2}) - \frac{u^{n+1} - u^n}{\Delta t} \right) + b^* \left(u(t^{n+1/2}), u(t^{n+1/2}), v_h \right)$$
$$- b^* \left(\frac{3}{2} u^n - \frac{1}{2} u^{n-1}, u^{n+1/2}, v_h \right) + \nu (\nabla(u(t^{n+1/2}) - u^{n+1/2}), \nabla v_h). \quad (4.13)$$

A priori estimates, from [18] for example, give us that

$$|\Phi(n, v_h)| \leq \frac{\nu}{4} \|\nabla v_h\|^2 + C\nu^{-1} \Delta t^4, \quad (4.14)$$

for a constant C dependent on norms of the NSE solution, but independent of h and Δt. Writing $e^n = u^n - w_h^n + w_h^n - u_h^n =: \eta^n + \phi_h^n$ for $w_h = P_{V_h}^{L^2}(u^n)$ (so $\eta^n \perp V_h$), then setting $v_h = \phi_h^{n+1/2}$ gives

$$\frac{1}{2\Delta t}(\|\phi_h^{n+1}\|^2 - \|\phi_h^n\|^2) + \nu \left\| \nabla \phi_h^{n+1/2} \right\|^2 + \gamma \left\| \nabla \phi_h^{n+1/2} \right\|^2 = \nu(\nabla \eta^{n+1/2}, \nabla \phi_h^{n+1/2})$$
$$+ \gamma g(\eta^{n+1/2}, \phi_h^{n+1/2}) - (p(t^{n+1/2}) - \gamma u_{1_x}^{n+1/2} - r_h, \nabla \cdot \phi_h^{n+1/2}) - b^* \left(\frac{3}{2} u_h^n - \frac{1}{2} u_h^{n-1}, \eta^{n+1/2}, \phi_h^{n+1/2} \right)$$
$$- b^* \left(\frac{3}{2} \eta^n - \frac{1}{2} \eta^{n-1}, u^{n+1/2}, \phi_h^{n+1/2} \right) - b^* \left(\frac{3}{2} \phi_h^n - \frac{1}{2} \phi_h^{n-1}, u^{n+1/2}, \phi_h^{n+1/2} \right) - \Phi(n, \phi_h^{n+1/2}), \quad (4.15)$$

where $r_h \in Q_h$ is arbitrary. Using $g(\eta, \phi) \leq C \|\nabla \eta\| \|\nabla \phi\|$, and applying standard upper bounds to the rest of the terms gives

$$\frac{1}{2\Delta t}(\|\phi_h^{n+1}\|^2 - \|\phi_h^n\|^2) + \nu \left\| \nabla \phi_h^{n+1/2} \right\|^2 + \gamma \left\| \nabla \phi_h^{n+1/2} \right\|^2 \leq C(\nu + \gamma^2 \nu^{-1} + \nu^{-1}) \left\| \nabla \eta^{n+1/2} \right\|^2$$
$$+ \gamma^{-1} \left\| p(t^{n+1/2}) - \gamma u_{1_x}^{n+1/2} - r_h \right\|^2 + C\nu^{-1} \left\| \nabla \left(\frac{3}{2} u_h^n - \frac{1}{2} u_h^{n-1} \right) \right\|^2 \left\| \nabla \eta^{n+1/2} \right\|^2$$
$$+ C\nu^{-1} \|u\|_{L^\infty(t^n, t^{n+1}; L^\infty(\Omega))}^2 (\|\phi_h^n\|^2 + \|\phi_h^{n-1}\|^2) + C\nu^{-1} \Delta t^4. \quad (4.16)$$

From here, standard techniques along with the use of the alternate Gronwall lemma from [14] (as is done in [15], since there are no ϕ_h^{n+1} appearing on the right hand side) completes the proof. $\square$

4.2 2d Channel Flow over a step

We now test the proposed method on the benchmark 2d problem of channel flow over a forward-backward facing step. The domain is taken to be a 40x10 rectangle, with a 1x1 step that is five units into the channel at the bottom. We prescribe no slipboundary conditions on all walls, and a parabolic inflow and outflow conditions given by $(y(10 - y)/25, 0)^T$. The correct physical behavior with $f = 0$ and $\nu = 1/600$ is a smooth velocity profile, with eddies forming and detaching behind the step [20]. A resolved NSE solution at T=40 is shown in figure 4, which is resolved using 21,593 degrees of freedom with $((P_2)^2, P_1)$ elements and a linearly extrapolated Crank-Nicolson timestepping with a timestep of $\Delta t = 0.01$ (note this is the scheme (4.8) with $\gamma = 0$), and we note this matches well the solution found in [20].

We test the proposed scheme on a coarser mesh, where the unstabilized NSE is not resolved. Here, we again use $((P_2)^2, P_1)$ Taylor-Hood elements, but on a mesh that provides only 4,780 degrees
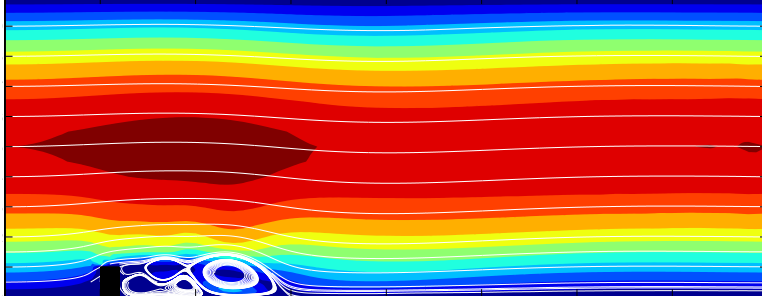
Figure 4: Shown above is the resolved NSE solution at T=40.

of freedom, and we keep all other problem parameters the same. A plot of the unstabilized NSE at T=40 is shown in Figure 5 (top) as velocity streamlines over speed contours as well as divergence contours, and it is observed that the solution is clearly incorrect, as significant oscillations are present in the speed contours. Results for the proposed scheme (4.8) with $\gamma = 1$ are shown for T=40 in Figure 5 (middle). Here the proposed stabilization operator is observed to create a dramatic increase in accuracy over the unstabilized solution, as there are no oscillations, and the streamlines match those of the true solution quite well. We also ran the same test using usual grad-div stabilization (with stabilization parameter 1) instead of the proposed divergence stabilization. The T=40 solution for this test is also shown in Figure 5, and we observe that its solution looks nearly identical to that found using the proposed stabilization. From the divergence contour plots, we observe that solution from both the new stabilization operator and the usual grad-div stabilization reduce the divergence error by an order of magnitude.

4.3   2D Flow around a cylinder

Next, we test the proposed method on two dimensional channel flow around a cylinder, which is a well studied problem often used in benchmarking for NSE algorithms [26, 17]. The flow patterns are driven by interaction of the fluid with the (solid wall) cylinder, which is an important scenario for many industrial flows. The domain is a 2.2×0.41 rectangular channel with a cylinder centered at $(0.2, 0.2)$ with radius 0.05. No slip boundary conditions are enforced on all walls, and the inflow and outflow profiles are set as

$$u_1(0, y, t) = u_1(2.2, y, t) = \frac{6}{0.41^2} \sin(\pi t/8) y(0.41 - y) \,,$$
$$u_2(0, y, t) = u_2(2.2, y, t) = 0.$$

The viscosity is taken to be $\nu = 10^{-3}$, and the external force $f = 0$. The flow is started from rest, and run to T=8. The correct behavior is for a vortex street to start to form behind the cylinder by T=4, and to persist through time T=8, as shown in [17].

We computed solutions using Algorithm 4.1 with timestep $\Delta t = 0.001$ and $((P_2)^2, P_1)$ Taylor-Hood elements on two different meshes, which provided 32,606, and 56,189 total degrees of freedom respectively. We ran the tests with $\gamma =0$ and 1 with the proposed divergence stabilization, and for comparison, with usual grad-div stabilization (with stabilization parameter 1). Plots of the velocity solution from the finest mesh at times T=4,6,7,8 using $\gamma = 1$ are shown in Figure 7, and agree well

No stabilization

Proposed stabilization with g
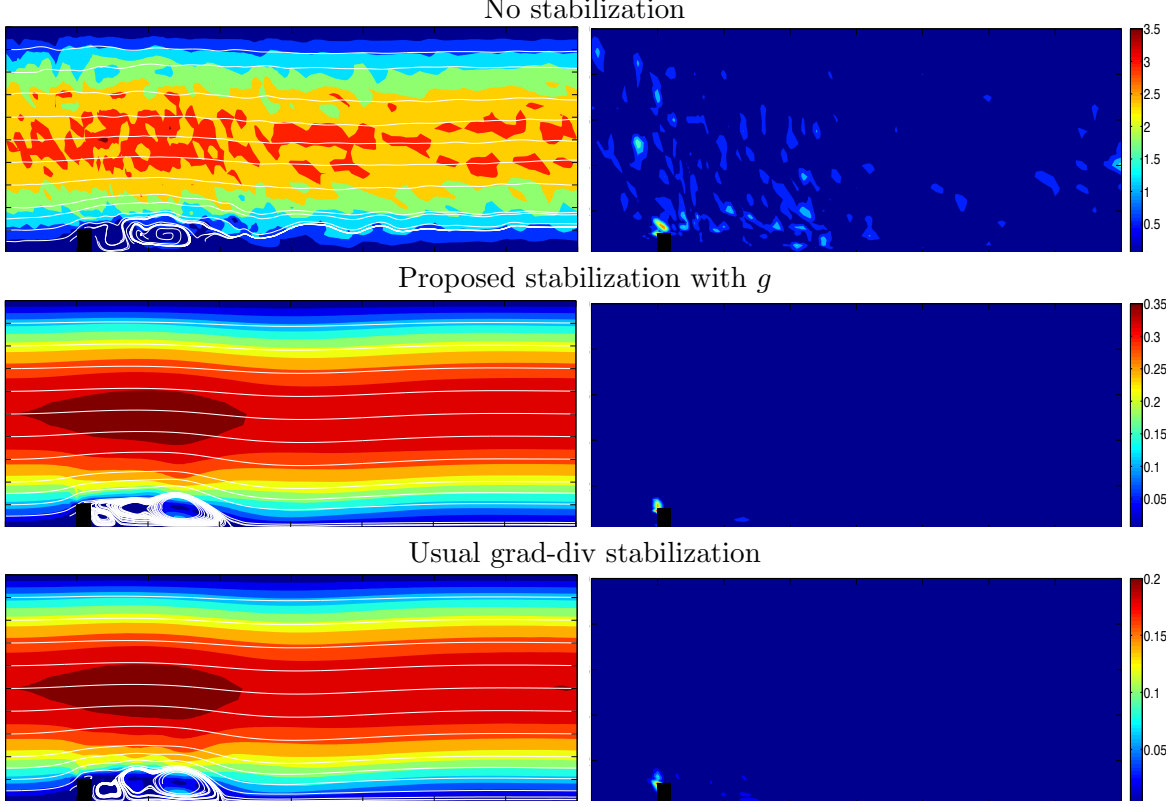
Usual grad-div stabilization

Figure 5: Shown above are the (left) velocity streamlines over speed contours and (right) absolute divergence $|\nabla \cdot u_h|$ contours for varying stabilizations.
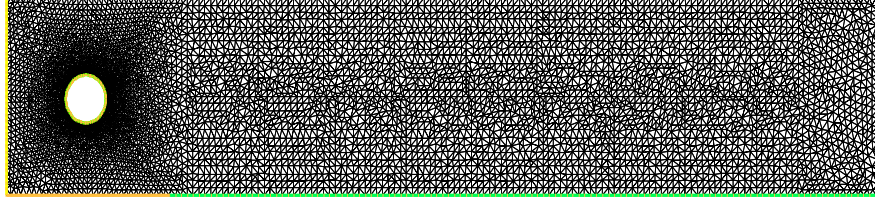

Figure 6: Shown above is the mesh used for the two dimensional flow past a cylinder numerical experiment, which provided 56,189 total degrees of freedom when used with $((P_2)^2, P_1)$ elements.

with those of the benchmark paper [17]. Plots of the solutions from the other meshes and other stabilization choices yielded similar plots.

To further evaluate and compare the computed solutions, we compute values for the maximal drag $c_{d,max}$ and lift $c_{l,max}$ coefficients at the cylinder, and compare them to those found in the benchmark tests that used over 1 million degrees of freedom and timesteps as small as 0.0001 [17]. The benchmark lift and drag coefficients for fully resolved NSE flows will lie in the reference intervals ([26, 17])

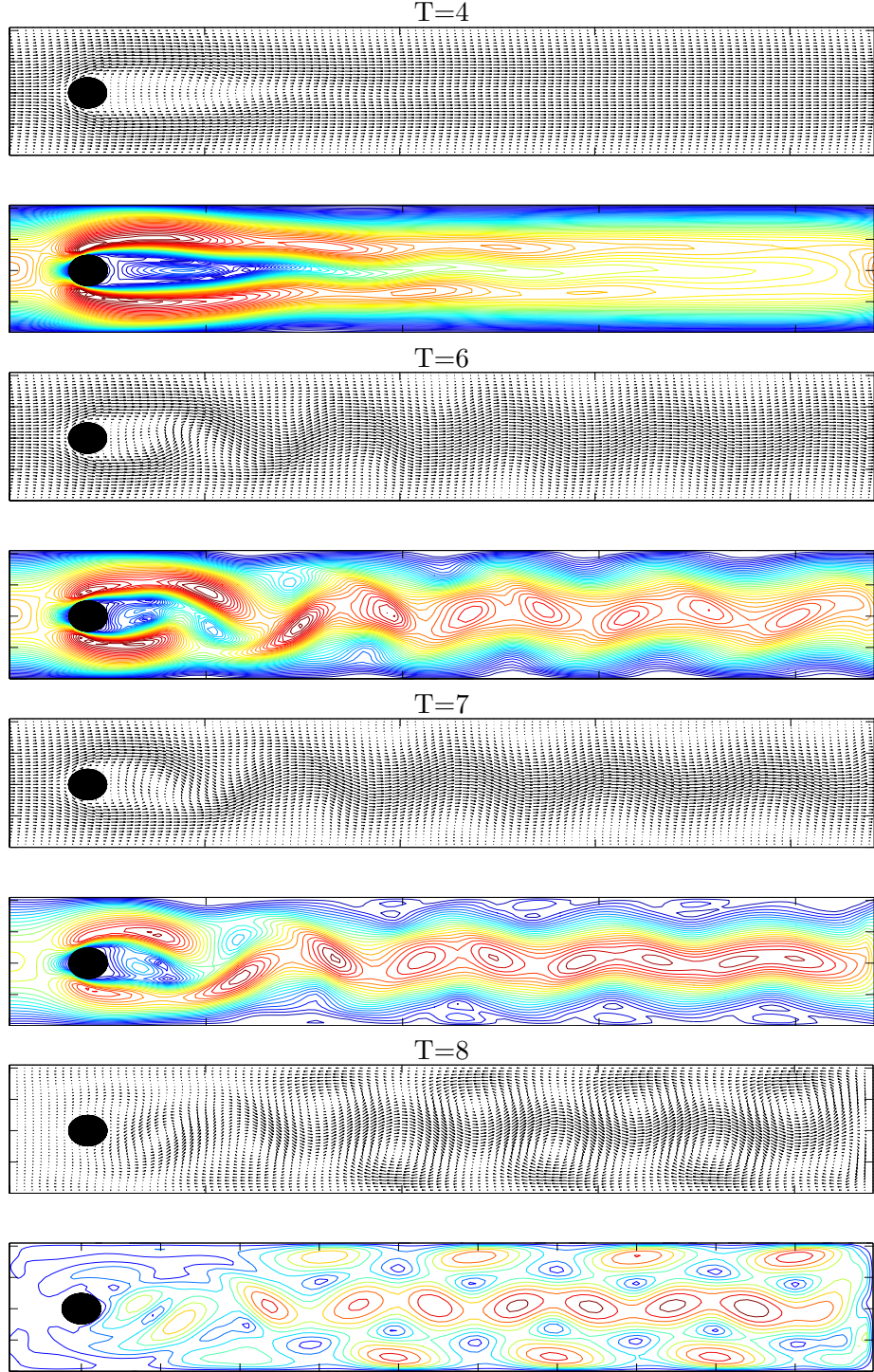$$c_{d,max}^{ref} \in [2.93, 2.97], \quad c_{l,max}^{ref} \in [0.47, 0.49].$$

18

Figure 7: Shown above are the velocity vector plots and speed contours for the 2d flow around a cylinder benchmark problem, at T=4, 6, 7, and 8, using the proposed divergence stabilization operator with $\gamma = 1$.

19

In table 4, we show the calculated lift and drag coefficients from our numerical tests. On the finest mesh, we observe that all solutions produced lift and drag coefficients in the reference intervals. However, on the coarser mesh, we observe that the stabilized solutions gave coefficients much closer to the reference intervals. We note again there is little difference between the solutions stabilized using the proposed divergence stabilization and usual grad-div stabilization.

	New stabilization		Grad-div stabilization		No stabilization	
dof	$c_{d,max}$	$c_{l,max}$	$c_{d,max}$	$c_{l,max}$	$c_{d,max}$	$c_{l,max}$
32,606	2.920	0.450	2.916	0.457	3.665	0.677
56,189	2.940	0.480	2.935	0.470	2.961	0.479

Table 4: Max lift and drag coefficients for 2d flow around a cylinder simulations, using various meshes and stabilizations.

4.4 The 3d Ethier-Steinman problem

Our final experiment is for computing approximations to the Ethier-Steinman exact NSE solution from [9], on $[0,1]^3$. For chosen parameters a, d and viscosity ν, this exact NSE solution is

$$u_1 = -a\left(e^{ax}\sin(ay+dz) + e^{az}\cos(ax+dy)\right)e^{-\nu d^2 t}, \tag{4.17}$$

$$u_2 = -a\left(e^{ay}\sin(az+dx) + e^{ax}\cos(ay+dz)\right)e^{-\nu d^2 t}, \tag{4.18}$$

$$u_3 = -a\left(e^{az}\sin(ax+dy) + e^{ay}\cos(az+dx)\right)e^{-\nu d^2 t}, \tag{4.19}$$

$$\begin{aligned} p = &-\frac{a^2}{2}(e^{2ax} + e^{2ay} + e^{2az} + 2\sin(ax+dy)\cos(az+dx)e^{a(y+z)} \\ &+ 2\sin(ay+dz)\cos(ax+dy)e^{a(z+x)} \\ &+ 2\sin(az+dx)\cos(ay+dz)e^{a(x+y)})e^{-2\nu d^2 t}. \end{aligned} \tag{4.20}$$

This problem is a 3d analog to the Green-Taylor vortex problem, for the purpose of benchmarking. Although unlikely to be physically realized, it is a good test problem because it is not only an exact NSE solution, but also it has non-trivial helicity which implies the existence of some turbulent structure [21] in the velocity field. We compute approximations using $a = 1$, $d = 1$, viscosity $\nu = 0.002$, timestep $\Delta t = 0.01$, endtime $T = 1$, and initial velocity $u^0 = (u_1(0), u_2(0), u_3(0))^T$, using Algorithm 4.1 with $((P_2)^3, P_1)$ elements on a tetrahedral mesh that provided 112,724 total degrees of freedom. Dirichlet boundary conditions we enforced nodally using the true solution, on all sides of the box. We computed using $\gamma = 0$ and 1, and plot $H^1(\Omega)$ spacial error vs. time for both computed solutions in Figure 8. A clear reduction of error is observable for the $\gamma = 1$ solution.

5 Conclusions and future directions

A new divergence stabilization operator for finite element simulations of incompressible flow problems has been introduced, which behaves in many ways like the well-known grad-div stabilization operator, but the new operator has the advantage of a sparser block structure in its linear algebraic system. By interpreting the new operator as grad-div stabilization together with the gradient of u_{1_x} (for example), analysis was given for finite element approximations of Stokes and NSE that showed the new operator maintains optimal convergence of standard finite element methods, penalizes the
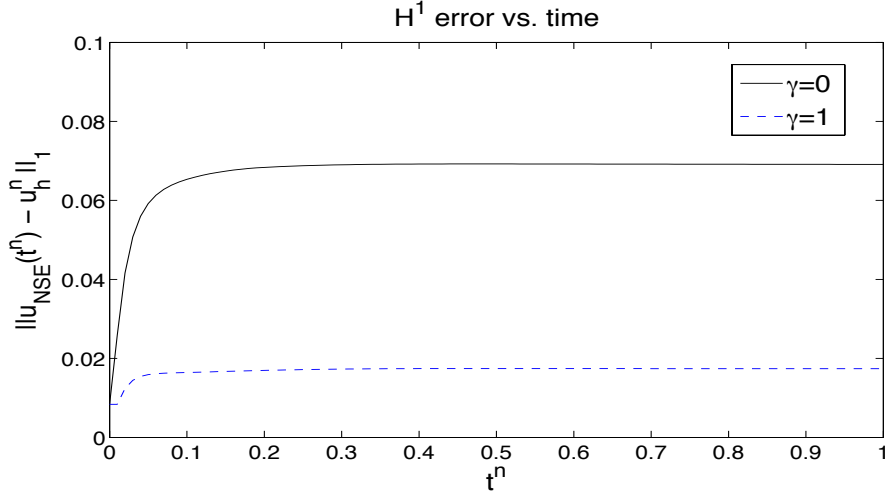
Figure 8: H^1 error vs. time, for solutions using $\gamma = 0$ and 1, to approximate the solution of the Ethier-Steinman problem with $a = d = 1$ and $\nu = 0.002$.

divergence error and can reduce the effect of the pressure error on the velocity error. Several benchmark numerical tests were performed which verified the theory, and showed the (sometimes dramatic) positive effect the proposed operator can have on solution accuracy.

Important future directions for the proposed stabilization operator are detailed studies of algebraic solvers for the linear systems that arise from the use of g. In particular, Chorin-type projection methods appear to be well suited to use the proposed operator (as opposed to usual grad-div), and so this seems to be a natural next step. For preconditioners and solvers that augment the Lagrangian, it may be interesting to study whether the new stabilization operator can be used together with the augmentation to achieve a better balance of accuracy and efficiency, since here the stabilization and augmentation parameters will be different.

References

[1] D. Arnold and J. Qin. Quadratic velocity/linear pressure Stokes elements. In R. Vichnevetsky, D. Knight, and G. Richter, editors, Advances in Computer Methods for Partial Differential Equations VII, pages 28–34. IMACS, 1992.

[2] G. Baker. Galerkin approximations for the Navier–Stokes equations. Harvard University, August 1976.

[3] M. Benzi and M. Olshanskii. An augmented Lagrangian-based approach to the Oseen problem. SIAM Journal of Scientific Computing, 28(6):2095–2113, 2006.

[4] S. Brenner and L. R. Scott. The Mathematical Theory of Finite Element Methods. Springer-Verlag, 1994.

[5] Jesús Carrero, Bernardo Cockburn, and Dominik Schötzau. Hybridized globally divergence-free LDG methods. I. The Stokes problem. Math. Comp., 75(254):533–563 (electronic), 2006.

[6] M. Case, V. Ervin, A. Linke, and L. Rebholz. A connection between Scott-Vogelius elements and grad-div stabilization. SIAM Journal on Numerical Analysis, 49(4):1461–1481, 2011.

[7] Bernardo Cockburn, Guido Kanschat, and Dominik Schötzau. A note on discontinuous Galerkin divergence-free solutions of the Navier-Stokes equations. J. Sci. Comput., 31(1-2):61–73, 2007.

[8] O. Dorok, W. Grambow, and L. Tobiska. Aspects of finite element discretizations for solving the Boussinesq approximation of the Navier-Stokes Equations. Notes on Numerical Fluid Mechanics: Numerical Methods for the Navier-Stokes Equations. Proceedings of the International Workshop held at Heidelberg, October 1993, ed. by F.-K. Hebeker, R. Rannacher and G. Wittum, 47:50–61, 1994.

[9] C. Eithier and D. Steinman. Exact fully 3d Navier-Stokes solutions for benchmarking. International Journal for Numerical Methods in Fluids, 19(5):369–375, 1994.

[10] L. Franca. Incompressible flows based upon stabilized methods. Notes on Numerical Fluid Mechanics, Proceedings of the International Workshop on Numerical Methods for the Navier-Stokes equations, Heidelberg, October, 1993.

[11] K. Galvin, A. Linke, L. Rebholz, and N. Wilson. Stabilizing poor mass conservation in incompressible flow problems with large irrotational forcing and application to thermal convection. Computer Methods in Applied Mechanics and Engineering, 237:166–176, 2012.

[12] P. Gresho and R. Sani. Incompressible Flow and the Finite Element Method, volume 2. Wiley, 1998.

[13] T. Heister and G. Rapin. Efficient augmented Lagrangian-type preconditioning for the Oseen problem using grad-div stabilization. Int. J. Numer. Meth. Fluids, 71:118134, 2013.

[14] J. Heywood and R. Rannacher. Finite element approximation of the nonstationary Navier-Stokes problem. Part IV: Error analysis for the second order time discretization. SIAM J. Numer. Anal., 2:353–384, 1990.

[15] R. Ingram. Unconditional convergence of high-order extrapolations of the Crank-Nicolson, finite-element method for the Navier-Stokes equations. Technical report, University of Pittsburgh, 2011.

[16] E. Jenkins, V. John, A. Linke, and L. Rebholz. On the parameter choice in grad-div stabilization for incompressible flow problems. Submitted, 2013.

[17] V. John. Reference values for drag and lift of a two dimensional time-dependent flow around a cylinder. International Journal for Numerical Methods in Fluids, 44:777–788, 2004.

[18] W. Layton. An Introduction to the Numerical Analysis of Viscous Incompressible Flows. SIAM, Philadelphia, 2008.

[19] W. Layton, C. Manica, M. Neda, M. A. Olshanskii, and L. Rebholz. On the accuracy of the rotation form in simulations of the Navier-Stokes equations. Journal of Computational Physics, 228(9):3433–3447, 2009.

[20] W. Layton, C. Manica, M. Neda, and L. Rebholz. Numerical analysis and computational testing of a high accuracy Leray-deconvolution model of turbulence. Numerical Methods for Partial Differential Equations, 24(2):555–582, 2008.

[21] H. Moffatt and A. Tsoniber. Helicity in laminar and turbulent flow. Annual Review of Fluid Mechanics, 24:281–312, 1992.

[22] M. A. Olshanskii. A low order Galerkin finite element method for the Navier-Stokes equations of steady incompressible flow: a stabilization issue and iterative methods. Comput. Meth. Appl. Mech. Eng., 191:55155536, 2002.

[23] M. A. Olshanskii, G. Lube, T. Heister, and J. Löwe. Grad-div stabilization and subgrid pressure models for the incompressible Navier-Stokes equations. Comput. Methods Appl. Mech. Engrg., 198(49-52):3975–3988, 2009.

[24] M. A. Olshanskii and A. Reusken. Grad-Div stabilization for the Stokes equations. Math. Comp., 73:1699–1718, 2004.

[25] A. Prohl. On pressure approximation via projection methods for nonstationary incompressible Navier-Stokes equations. SIAM J. Numer. Anal., 47(1):158–180, 2009.

[26] M. Schäfer and S. Turek. The benchmark problem 'flow around a cylinder' flow simulation with high performance computers II. in E.H. Hirschel (Ed.), Notes on Numerical Fluid Mechanics, 52, Braunschweig, Vieweg:547–566, 1996.

[27] S. Zhang. A new family of stable mixed finite elements for the 3d Stokes equations. Math. Comp., 74(250):543–554, 2005.

[28] S. Zhang. On the family of divergence-free finite elements on tetrahedral grids for the Stokes equations. Preprint University of Delaware, 2007.

[29] S. Zhang. On the P1 Powell-Sabin divergence-free finite element for the Stokes equations. J. Comput. Math., 26(3):456–470, 2008.

[30] S. Zhang. Quadratic divergence-free finite elements on Powell-Sabin tetrahedral grids. Calcolo, 48(3):211–244, 2011.

[31] Shangyou Zhang. A family of $Q_{k+1,k} \times Q_{k,k+1}$ divergence-free finite elements on rectangular grids. SIAM J. Numer. Anal., 47(3):2090–2107, 2009.